ROYAL SOCIETY
OF CHEMISTRY

REVIEW

Check for updates

Emerging high voltage V^{4+}/V^{5+} redox reactions in $Na_3V_2(PO_4)_3$-based cathodes for sodium-ion batteries

Meng Zhou,†[a] Xunzhu Zhou,†[bc] Lin Li, [ID] *[bcd] Xiang Chen,[e] Zhenan Qiao [ID] *[d] and Shulei Chou [ID] *[bc]

$Na_3V_2(PO_4)_3$ (NVP) cathode materials with the advantages of long cycle life and superior thermal stability have been considered promising cathode candidates for SIBs. However, the unsatisfactory energy density derived from low theoretical capacity and operating voltage (3.35 V *vs.* Na^+/Na, based on the V^{3+}/V^{4+} redox couple) inevitably limits their practical application. Therefore, the activation of the V^{4+}/V^{5+} redox couple (∼4.0 V *vs.* Na^+/Na) in NVP-based cathode materials to boost the energy density of SIBs has attracted extensive attention. Herein, we first analyze the challenges of activation of the V^{4+}/V^{5+} redox couple in NVP-based cathode materials. Subsequently, the recent achievement of NVP-based cathode materials with activated V^{4+}/V^{5+} redox reactions for SIBs is overviewed. Finally, further research directions of high voltage V^{4+}/V^{5+} redox reactions in NVP-based cathodes are proposed. This review provides valuable guidance for developing high energy density NVP-based cathode materials for SIBs.

1. Introduction

Since lithium-ion batteries (LIBs) were successfully commercialized by Sony in 1991, they have been widely applied in portable/mobile electronics (*e.g.* laptops, cell phones, *etc.*) and electric vehicle fields and exhibited a promising application in large-scale energy storage systems.[1–3] However, an unfortunate fact is, the element lithium (Li) is rare (20 ppm) and unevenly distributed on our planet.[4] Large-quantity applications of LIBs in EVs and large-scale energy storage systems will inevitably cause the depletion of lithium resources and will cause a steep increase in costs, which is unfavorable both ecologically and economically. Sodium, which shows similar physical and chemical properties to lithium, is the fifth-most abundant element in the earth's crust. The earth-abundant properties of sodium make sodium-ion batteries (SIBs) ideal supplements for

LIBs, especially with great prospects for application in large-scale energy storage systems.[5–9]

The working principle of SIBs is similar to that of LIBs. During the charging process, Na^+ is released from the cathode and embedded into the anode through the electrolyte. In order to balance the charge, the electrons move from the external circuit to the anode. While during discharging, it is completely the opposite. The electrode material plays a key role in the electrochemical performance of SIBs. For the anode materials, hard carbons (HCs) with a low void, highly disordered structure, large layer space and achievable reversible capacity above 300 mA h g^{-1}, are considered to be the most promising anode materials for SIBs and extensively applied both in laboratory research and the market.[10,11] As for the cathode side, the widely studied materials of SIBs at present are layered transition metal (TM) oxides,[12–15] polyanionic materials,[16–19] Prussian Blue[20–22] and organic materials.[23–25] Polyanionic materials, with a general formula of $Na_xM_y(X_aO_b)_zZ_w$ (where M represents one or more transition metals such as Ti, V, Cr, Mn, Fe, Co, Ni, *etc.*; X = Si, B, S, P, *etc.*; Z = F, OH, *etc.*), have been regarded as potential cathode materials for high performance SIBs due to the advantages of stable structure frameworks and superior safety.[16,26,27]

Among the reported polyanionic materials, NASICON-structured $Na_3V_2(PO_4)_3$ (NVP) became the most typical polyanionic material and received extensive attention in SIBs.[28,29] Typically, the multivalent vanadium atom allows a consecutive redox reaction of $V^{2+}/V^{3+}/V^{4+}/V^{5+}$, with a considerable energy output. According to the previous reports, NVP generally undergoes a two-electron reaction (V^{3+}/V^{4+}) during the charge/

[a]*College of Chemical Engineering and Technology, Yantai Nanshan University, Yantai, Shandong 265713, China*

[b]*Institute for Carbon Neutralization Technology, College of Chemistry and Materials Engineering, Wenzhou University, Wenzhou, Zhejiang 325035, China. E-mail: linli@wzu.edu.cn; chou@wzu.edu.cn*

[c]*Wenzhou Key Laboratory of Sodium-Ion Batteries, Wenzhou University Technology Innovation Institute for Carbon Neutralization, Wenzhou, Zhejiang 325035, China*

[d]*State Key Laboratory of Inorganic Synthesis and Preparative Chemistry, College of Chemistry, Jilin University, Changchun 130012, P. R. China. E-mail: qiaozhenan@jlu.edu.cn*

[e]*College of Textile Science and Engineering (International Institute of Silk), Zhejiang Sci-Tech University, Hangzhou 310018, PR China*

† These authors contributed equally: Meng Zhou and Xunzhu Zhou.

discharge process, obtaining an operating voltage of 3.35 V (vs. Na^+/Na) and a reversible capacity of 110 mA h g^{-1}.[30] It seems impossible for NVP to extract more than 2 Na^+ to realize the reversible transition of the V^{4+}/V^{5+} redox couple, accompanied by the phase transition from $NaV_2(PO_4)_3$ to $V_2(PO_4)_3$.[31] Therefore, it is worth noting that the successful activation of the V^{4+}/V^{5+} redox couple is of vital importance in the electrochemical performance of SIBs, for it not only gives an elevated electrochemical platform ($\sim$4.0 V), but also offers additional capacity, and thus, a significantly enhanced energy density for NVP-based cathode materials (Fig. 1a).[32,33] Until now, multiple advancements in the activation of the V^{4+}/V^{5+} redox couple in NVP-based cathode materials have been achieved (Fig. 1b). To the best of our knowledge, there are currently no relevant reviews in this field.

In this review, we will focus on the cation substituted NVP-based cathodes with triggered V^{4+}/V^{5+} redox reactions to improve the energy density of SIBs. We first introduced the challenges of NVP-based cathodes to achieve reversible activation of the V^{4+}/V^{5+} redox couple. Then, we overviewed the recent achievements of NVP-based cathodes with activated V^{4+}/V^{5+} redox reactions. Finally, future perspectives on activating V^{4+}/V^{5+} redox reactions in NVP-based cathode materials for SIBs will also be highlighted.

2. Challenges of activation of the V^{4+}/V^{5+} redox couple

According to the density functional theory (DFT) calculations, pure NVP exhibits a high V^{4+}/V^{5+} redox potential of 4.64 V, which is beyond the electrochemical window of most electrolytes.[34] Therefore, the V^{4+}/V^{5+} redox reaction can barely be activated in $Na_3V_2(PO_4)_3$. In general, transition metal substitution was demonstrated as an effective strategy to activate the V^{4+}/V^{5+} redox reaction in NVP-based cathode materials. However, for NASICON-structured NVP-based cathode materials with the activated V^{4+}/V^{5+} redox couple, there still exist some

challenges that limit their practical application, including low electronic conductivity and unsatisfactory structure reversibility at high voltage.[35,36] In general, NASICON-structured NVP-based materials exhibit acceptable Na^+ ionic conductivity due to their unique 3D open framework for fast ionic transfer. However, the intrinsically low electronic conductivity inevitably leads to sluggish electrochemical reaction kinetics, causing inferior rate performance. In addition, more Na^+ intercalation/deintercalation into/from NVP-based cathode materials with the activated V^{4+}/V^{5+} redox couple results in a relatively large volume change during the charge/discharge process, which leads to structure collapse and poor cycling stability. Therefore, it's important to explore NVP-based cathode materials with stable structure frameworks and high electronic conductivity for highly reversible activation of the V^{4+}/V^{5+} redox couple.

3. Recent achievement of activation of the V^{4+}/V^{5+} redox couple

3.1 Single metal substitution

In 2015, Tirado's group first disclosed the V^{4+}/V^{5+} redox reaction in NVP-based cathode materials.[37] A series of Fe^{3+} substituted NVP ($Na_3V_{2-x}Fe_x(PO_4)_3$, $0 \leq x \leq 0.5$) materials was prepared through a simple sol–gel method. Fe-substituted materials ($x \geq 0.2$) showed an obvious redox peak at ca. 4 V, corresponding to the V^{4+}/V^{5+} redox reaction, which is demonstrated using the XPS and ^{57}Fe Mössbauer spectra. Attempt on substitution of the V site with aliovalent Fe^{2+} to obtain sodium-rich compounds was first proposed by Yamada's group.[38] The Na-rich composite $Na_{3.5}V_{1.5}{}^{3+}Fe_{0.5}{}^{2+}(PO_4)_3$ delivers a capacity retention of 80% after 300 cycles. Subsequently, a novel sodium-deficient NASICON material $Na_{3.41}\pounds_{0.59}FeV(PO_4)_3$ was applied in SIBs.[39] $Na_{3.41}\pounds_{0.59}FeV(PO_4)_3$ shows a high initial discharge capacity of 170 mA h g^{-1} with three electron reactions in the wide voltage of 1.5–4.4 V. In addition, $Na_{3.41}\pounds_{0.59}FeV(PO_4)_3$ shows a single-phase mechanism with a small volume change of 3.44% during the charge/discharge process, which is responsible for
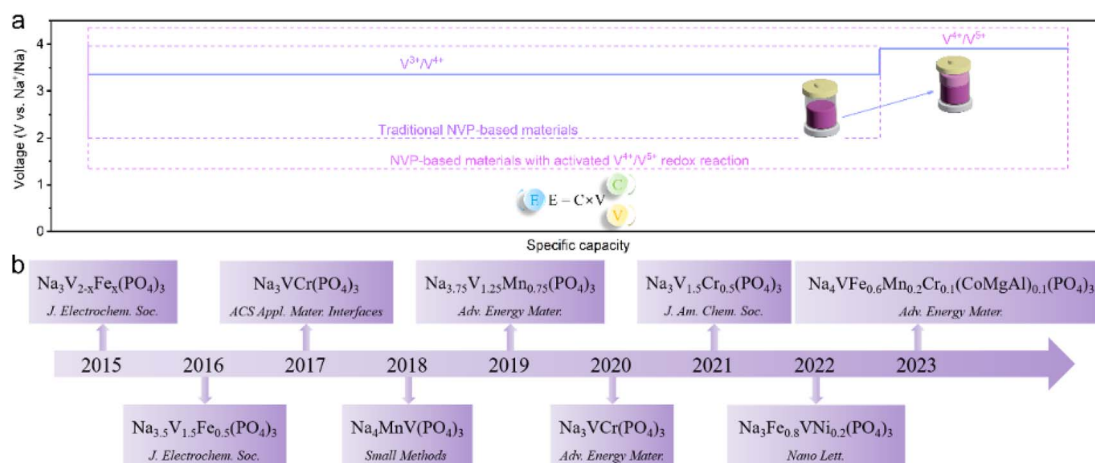

Fig. 1 (a) Schematical illustration of the advantages of NVP-based materials with the activated V^{4+}/V^{5+} redox reaction. (b) Timeline of the progress of high voltage V^{4+}/V^{5+} redox reactions in NVP-based cathodes.
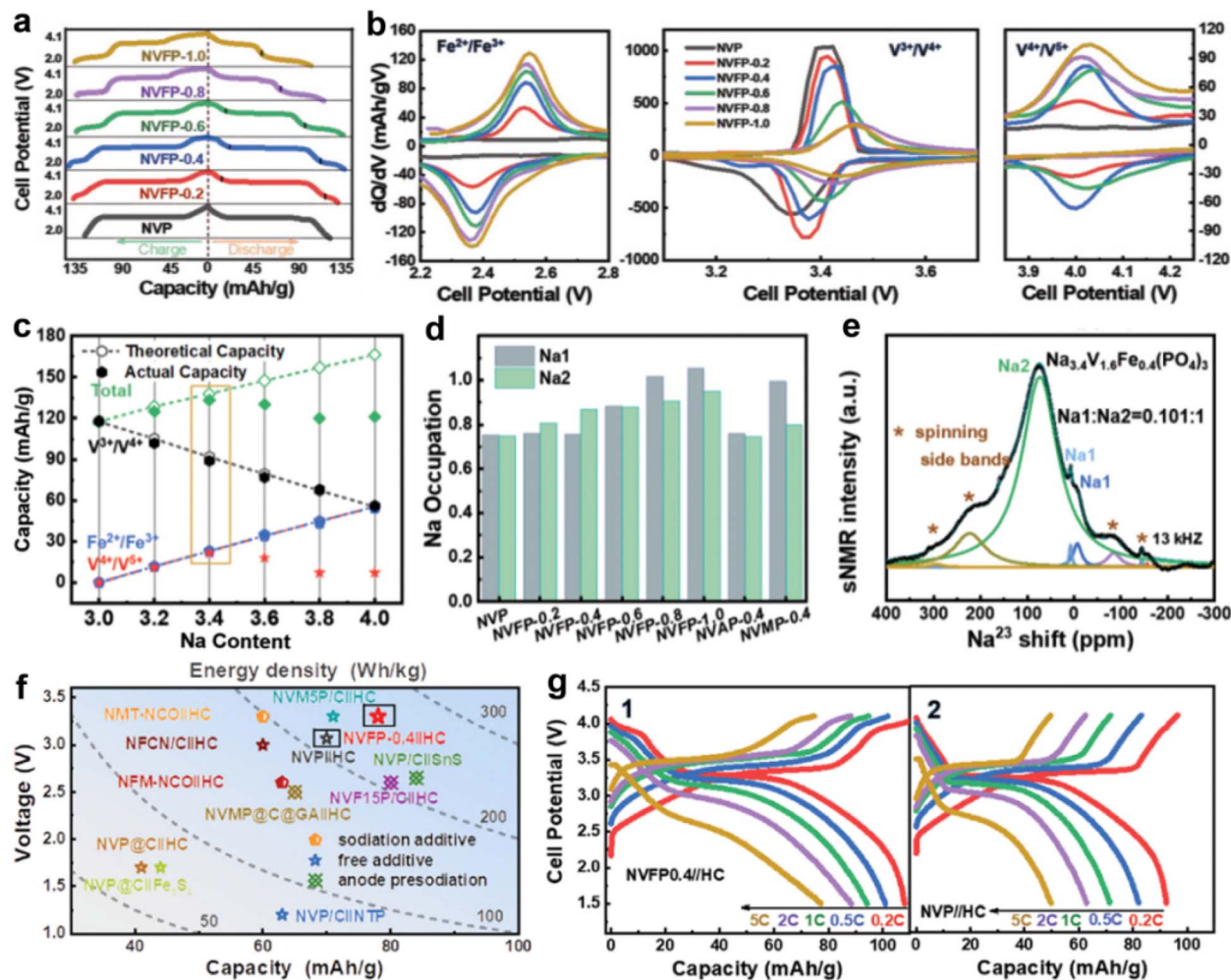
Fig. 2 (a) The charge/discharge curves of pure NVP and NVFP-x ($0 < x \leq 1$). (b) dQ/dV curves of Fe^{2+}/Fe^{3+}, V^{3+}/V^{4+}, and V^{4+}/V^{5+} redox reactions in pure NVP and Na-rich NVFP-x samples. (c) Comparison of the actual capacity and theoretical capacity of NVFP-x samples with different Na contents. (d) The Na occupations of the NVFP-x family according to XRD refinement. (e) The fitted ^{23}Na ss-NMR spectra of NVFP-0.4. (f) Comparison of the energy density of the state-of-the-art full cells for NIBs. (g) The charge/discharge curves of NVFP-0.4‖HC (g1) and NVP‖HC (g2) at different rates from 0.2 to 5C. Reproduced with permission.[40] Copyright 2022, Wiley-VCH.

its superior cycling stability. Recently, Hu's group prepared various carbon-coated Na-rich $Na_{3+x}V_{2-x}Fe_x(PO_4)_3$ (NVFP-x, where x = 0, 0.2, 0.4, 0.6, 0.8 and 1.0) cathodes for SIBs; Fe^{2+}/Fe^{3+} (2.45 V), V^{3+}/V^{4+} (3.35 V), and V^{4+}/V^{5+} (3.95 V) redox reactions were observed (Fig. 2a and b).[40] As shown in Fig. 2c, NVFP-0.4 has a highest actual capacity of ~133 mA h g^{-1} due to its highly reversible V^{4+}/V^{5+} (3.95 V) redox reactions. Noticeably, they uncovered that the relative contents of Na_1 and Na_2 in the structure play an important role in the reversibility of V^{4+}/V^{5+} redox couples, and enough Na_2 content is necessary to enable reversible activation (Fig. 2d and e). The Fe substitution is closely related to the Na content at the Na_2 site, and the Na_1/Na_2 ratio reached a minimum value when x = 0.4. Moreover, they proposed that the Na$^+$ ion extraction from NVFP-0.4 during the Fe^{2+}/Fe^{3+} redox reaction at low-voltage can act as the Na compensation agent in the NVFP-0.4‖HC full cells. As a result, the NVFP-0.4‖HC full cells show an improved energy density and rate performance, compared with NVP‖HC full cells (Fig. 2f

and g). The high efficiency, simple operation, and easily scalable feature of the Na self-compensation strategy can effectively promote the practical application of SIBs.

Most recently, $Na_{3.5}V_{1.5}Fe_{0.5}(PO_4)_3$ was reported by Liang's group, in which the reversible V^{4+}/V^{5+} redox reaction was activated with a capacity of 148.2 mA h g^{-1} and enabled an improved energy density.[41] A highly reversibly chemical state evolution of V and Fe (Fe^{2+}/Fe^{3+}, V^{3+}/V^{4+}, and V^{4+}/V^{5+}) during the charge/discharge process was demonstrated by XPS (Fig. 3a). Noticeably, they proposed that the reversible V^{4+}/V^{5+} redox reaction was dependent on the unpaired electrons of Fe in the 3d orbital (Fig. 3b and c). As shown in Fig. 3d and e, $Na_{3.5}V_{1.5}Fe_{0.5}(PO_4)_3$ shows a lower forbidden bandgap of 1.05 eV than that of $Na_3V_2(PO_4)_3$, indicating its improved electronic conductivity. In addition, $Na_{3.5}V_{1.5}Fe_{0.5}(PO_4)_3$ exhibits a low Na$^+$ migration energy barrier and fast Na$^+$ diffusion kinetics. Therefore, $Na_{3.5}V_{1.5}Fe_{0.5}(PO_4)_3$ shows an obvious advantage in terms of energy density (501 W h kg^{-1}) and rate performance.

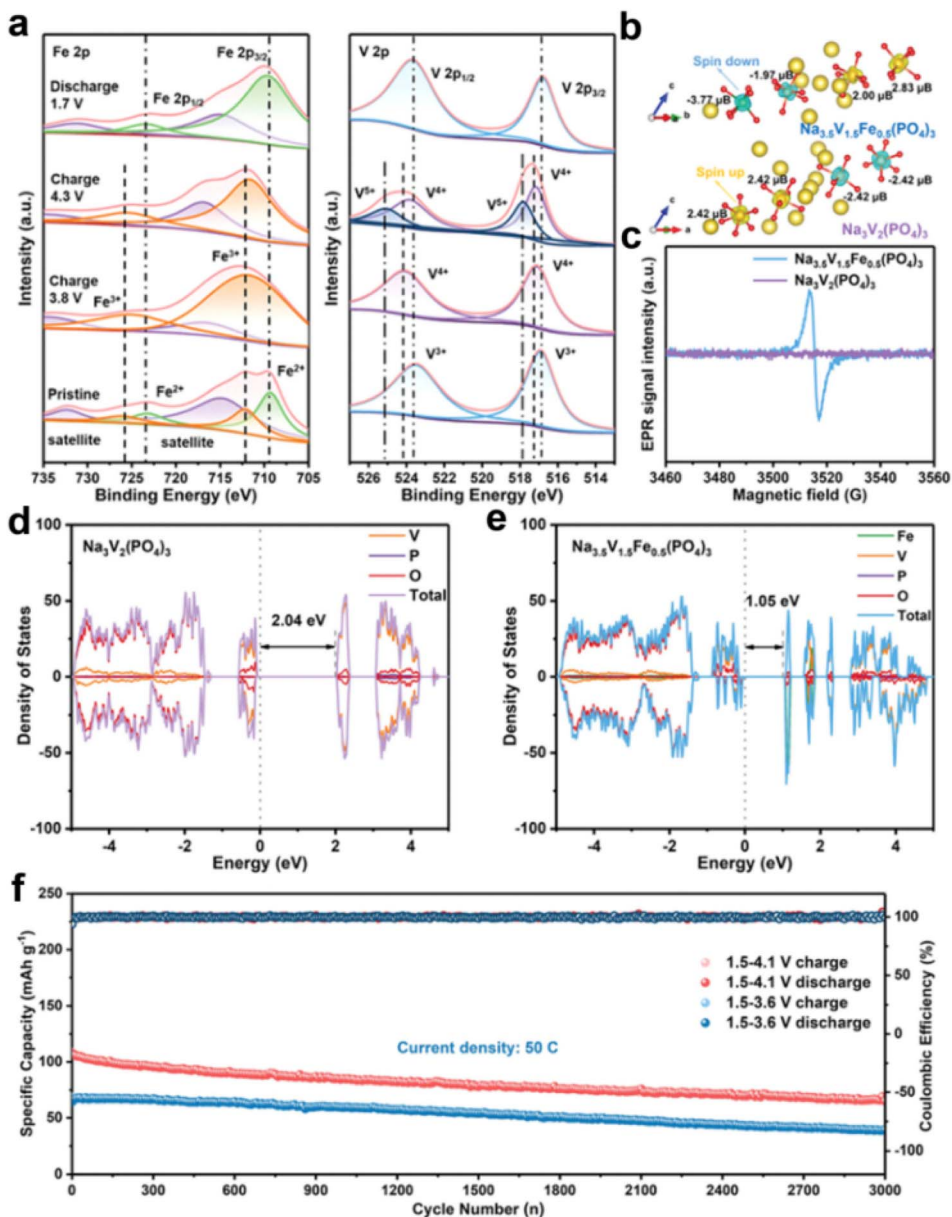Fig. 3 (a) XPS spectra of Fe and V at different electrochemical states for the $Na_{3.5}V_{1.5}Fe_{0.5}(PO_4)_3$ electrode. (b) The comparative electronic spin states and (c) EPR spectra of $Na_{3.5}V_{1.5}Fe_{0.5}(PO_4)_3$ and NVP. (d and e) DFT calculations of total DOS and the selected element DOS of (d) NVP and (e) $Na_{3.5}V_{1.5}Fe_{0.5}(PO_4)_3$. (f) Long-term cycling stability of the HC‖NVFP full cells. Reproduced with permission.[41] Copyright 2023, Wiley-VCH.

More importantly, the superior electrochemical performance of $Na_{3.5}V_{1.5}Fe_{0.5}(PO_4)_3$‖HC demonstrated the potential of $Na_{3.5}$-$V_{1.5}Fe_{0.5}(PO_4)_3$ for practical application (Fig. 3f). This work could significantly accelerate the commercialization of sodium-ion batteries.

The electrochemical performance of sodium-rich compounds of $Na_4MnV(PO_4)_3$ and $Na_4NiV(PO_4)_3$ was investigated by Goodenough's group.[42] However, no V^{4+}/V^{5+} redox reaction was observed in $Na_4MnV(PO_4)_3$ due to the low cut-off voltage of 3.8 V, which needs to be further explored in a wide voltage range. Noticeably, the Ni^{2+} and V^{4+} in $Na_4NiV(PO_4)_3$ were partially oxidized to Ni^{3+} and V^{5+} after charging to 4.2 V. Subsequently, Masquelier's group investigated the

electrochemical behavior of $Na_4MnV(PO_4)_3$ at a high cutoff voltage of 4.3 V.[36] $Na_4MnV(PO_4)_3$ delivers a high charge capacity of ~156 mA h g^{-1} with electrochemical oxidation of the V^{4+} state to the V^{5+} state. Unfortunately, operando X-ray diffraction revealed a irreversible structure evolution during the charge/discharge process, which resulted in an unsatisfactory cycling stability (Fig. 4a). Subsequently, Ghosh et al. performed a comprehensive study to understand the role of Mn^{2+} in NVP.[43] They found that the electrochemical performance of Mn-substituted NVP can be significantly improved by modulating electronic and crystal structures. $Na_{3.75}V_{1.25}Mn_{0.75}(PO_4)_3$ with an optimized bottleneck size (≈ 5 Å^2) and modulated V- and Mn-redox centers show highly reversible redox processes that
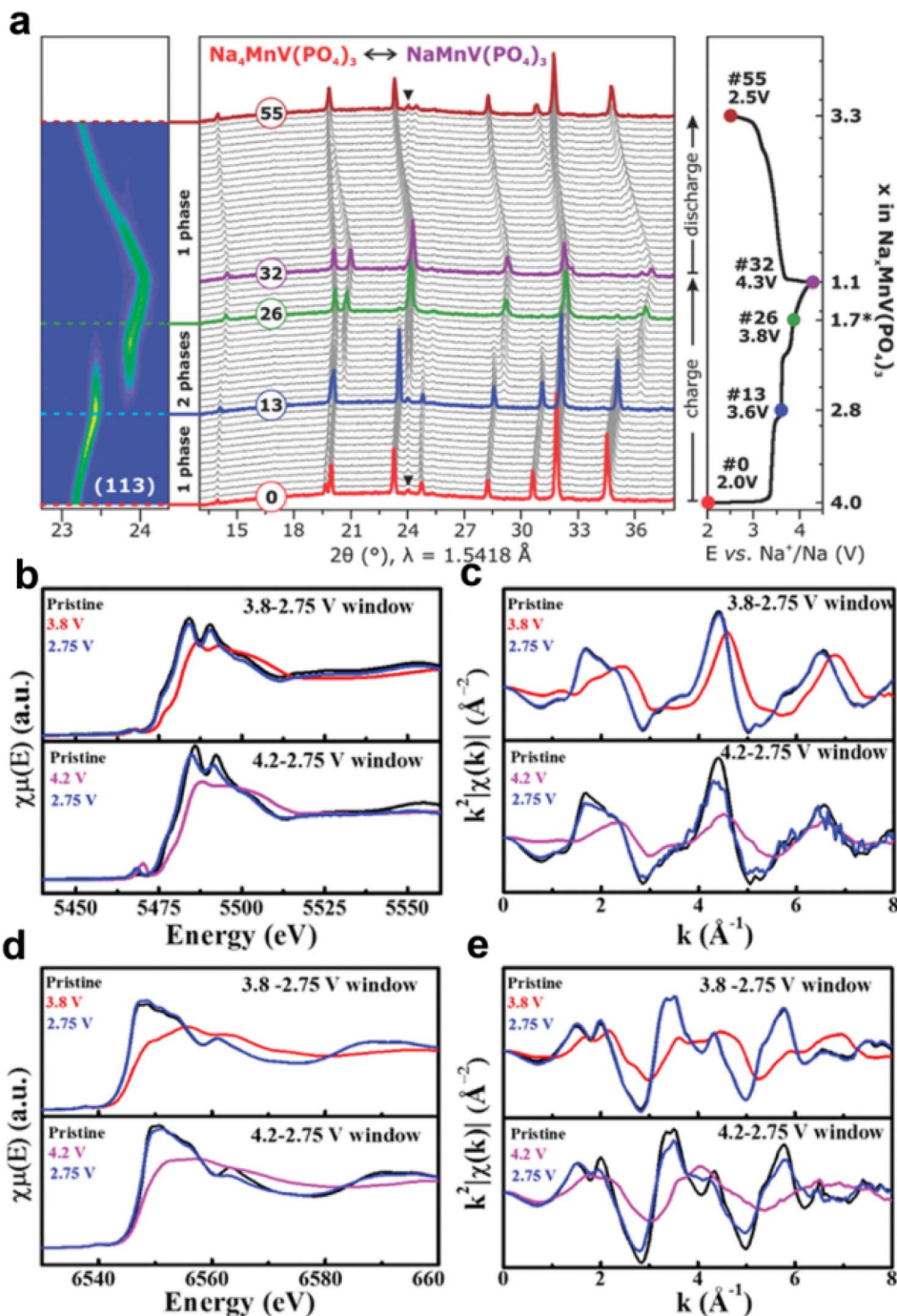
Fig. 4 (a) *Operando* XRD patterns of $Na_4MnV(PO_4)_3$ during the first cycle. Reproduced with permission.[36] Copyright 2019, Wiley-VCH. (b and d) *Ex situ* XAS of $Na_{3.75}V_{1.25}Mn_{0.75}(PO_4)_3$ cathodes at different states and the normalized absorption spectra at V- and Mn-K edges. (c and e) k^2-Weighted $\chi(k)$ signals collected at V-K and Mn-K edges. Reproduced with permission.[43] Copyright 2020, Wiley-VCH.

enable a better rate performance and cycling stability than that of $Na_4MnV(PO_4)_3$ (Fig. 4b–e).

The Mg-substitution strategy was proposed by Okada and coworkers; $Na_{3+x}V_{2-x}Mg_x(PO_4)_3$ ($x = 0.1$ to 0.7) was synthesized as a cathode material for SIBs.[44] Among these, $Na_{3.2}V_{1.8}Mg_{0.2}(PO_4)_3$ demonstrated a higher capacity (122 mA h g^{-1}) than undoped $Na_3V_2(PO_4)_3$ (117.6 mA h g^{-1}) because of the successful activation of the V^{5+}/V^{4+} redox couple. In contrast,

$Na_{3.5}V_{1.5}Mg_{0.5}(PO_4)_3$ shows a low discharge capacity due to the poor reversibility of the V^{5+}/V^{4+} redox couple, which derived from the irreversible change in the crystal structure when charged to 4.3 V.

The activation of the V^{4+}/V^{5+} redox couple in Cr^{3+} substituted NVP was first revealed by Lavela's group.[45] Subsequently, Yang's group investigated the electrochemical sodium storage behaviors of $Na_3VCr(PO_4)_3$ (NVCP) by a series of advanced
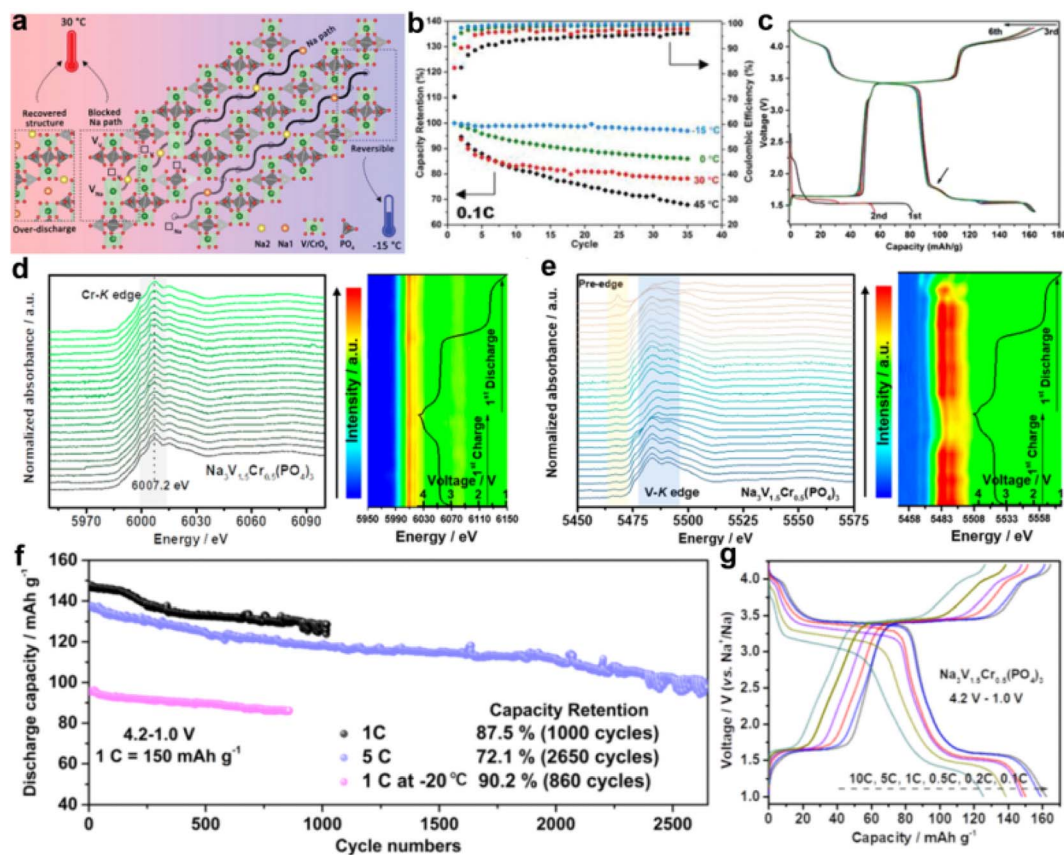
Fig. 5 (a) Schematic graphical illustration of the V migration in $Na_{2-x}VCP$ at 30 °C and −15 °C. (b) Charge/discharge capacity of $Na_3VCr(PO_4)_3$ (NVCP) electrodes cycled between 2.5 and 4.3 V at different temperatures at 0.1C. (c) Cycling results of the over-discharge method at 0.1C at 30 °C. First discharged to 1.4 V, cycled between 1.4 and 2.5 V in the second cycle, and then 1.4–4.3 V in subsequent cycles. Reproduced with permission.[35] Copyright 2021, Wiley-VCH. (d) *Operando* XANES spectra and 2D contour plot at the Cr-K edge and (e) V-K edge of the Na_3-$V_{1.5}Cr_{0.5}(PO_4)_3$ electrode for the first cycle. (f) Long-term cycling stability of the $Na_3V_{1.5}Cr_{0.5}(PO_4)_3$ electrode at 1C (at room temperature and at −20 °C) and 5C. (g) Galvanostatic charge/discharge curves of the $Na_3V_{1.5}Cr_{0.5}(PO_4)_3$ electrode at different rates. Reproduced with permission.[47] Copyright 2021, American Chemical Society.

characterization techniques such as *ex situ* ^{51}V solid-state nuclear magnetic resonance, X-ray absorption near-edge structure, and *in situ* X-ray diffraction.[46] They proposed that the poor cycling stability of NVCP at a high cutoff voltage of 4.3 V at 30 °C originates from the irreversible structure evolution and uncovered local environment of vanadium atoms. Noticeably, decreasing the testing temperature was demonstrated as an effective way to suppress the irreversible structure evolution and boost the electrochemical performance. NVCP exhibits improved cycling stability (a capacity retention of 92% after 200 cycles) at −15 °C. The structural degradation mechanism of NVCP was further explored by combining with *in situ* XRD, *ex situ* X-ray absorption fine structure (XAFS) at the V-K edge, *ex situ* soft X-ray absorption spectroscopy (sXAS) at the V-L edge and atomically resolved electron microscopy.[35] They found that the V migration during deep Na^+ extraction induces irreversible structural transformation of NVCP at 30 °C (Fig. 5a). Therefore, relieving diffusion of V atoms by decreasing the operating temperature is an effective method to improve the structural stability of NVCP (Fig. 5b). In addition, they proposed a more practical strategy to boost the sodium storage performance of

NVCP. The collapsed structure can be restored by room temperature low voltage discharging (<1.7 V), which can make dislocated V atoms return to their original lattice. Therefore, the capacity decay of NVCP was suppressed in a wide voltage range of 1.7–4.3 V (Fig. 5c).

$Na_3V_{1.5}Cr_{0.5}(PO_4)_3$ was reported by Goodenough and coworkers, which delivers a high capacity of 150 mA h g^{-1} with reversible three-electron redox reactions (V^{2+}/V^{3+} at 1.6 V, V^{3+}/V^{4+} at 3.6 V, and V^{4+}/V^{5+} at 4.1 V) and an excellent cycling stability (96% capacity retention after 400 cycles).[32] Benefiting from the potential difference between the three redox couples in $Na_3V_{1.5}$-$Cr_{0.5}(PO_4)_3$, a symmetric sodium-ion battery was assembled. The symmetric cell maintained a specific capacity of ~100 mA h g^{-1} after 200 cycles and a capacity of 75 mA h g^{-1} at 1 A g^{-1}. The structural and electrochemical behaviors of $Na_3V_{1.5}Cr_{0.5}(PO_4)_3$ were comprehensively investigated by Kang's group.[47] The unique solid-solution reaction of $Na_3V_{1.5}Cr_{0.5}(PO_4)_3$ was demonstrated by *operando* XRD. As shown in Fig. 5d and e, the V^{4+}/V^{5+} redox couple was activated in $Na_3V_{1.5}Cr_{0.5}(PO_4)_3$, and the Cr is maintained electrochemically inactive during the charge/discharge process. The Cr substitution achieves a lower sodium
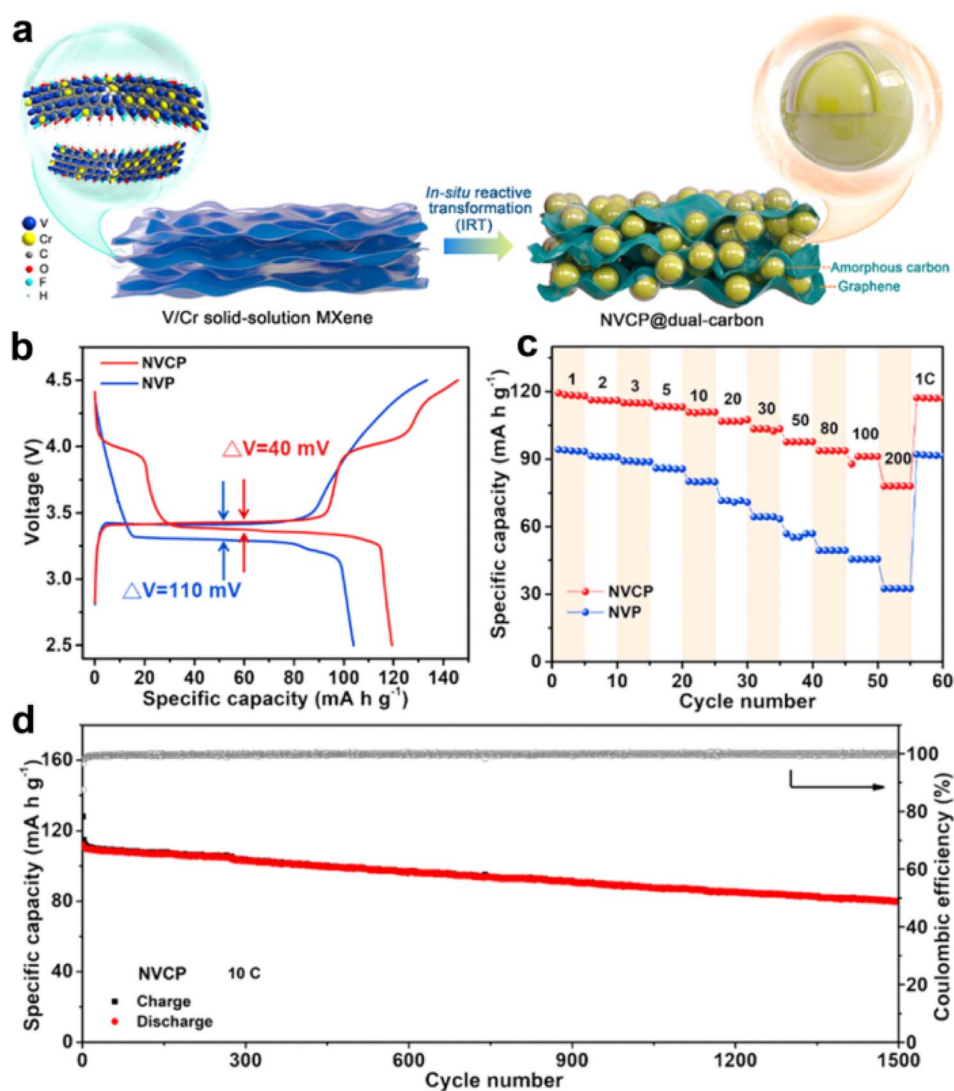
Fig. 6 (a) Schematic representation of the *in situ* reactive transformation of MXene to $Na_3V_{1.625}Cr_{0.375}(PO_4)_3$@dual-carbon architectures. (b) The charge/discharge curves of NVP and $Na_3V_{1.625}Cr_{0.375}(PO_4)_3$. (c) Comparison of rate capability of $Na_3V_{1.625}Cr_{0.375}(PO_4)_3$ and NVP. (d) Long-term cycling stability of NVCP. Reproduced with permission.[49] Copyright 2022, American Chemical Society.

diffusion barrier of 0.311 eV and a smaller forbidden bandgap of 1.98 eV, compared with NVP. Benefiting from the above merits, $Na_3V_{1.5}Cr_{0.5}(PO_4)_3$ delivers a high reversible capacity (163.2 mA h g^{-1} at 0.1C), long cycle life (a capacity retention of 72.1% even after 2650 cycles, Fig. 5f), superior rate performance (~127 mA h g^{-1} at 10C, Fig. 5g) and good low-temperature performance (a reversible capacity of 97.5 mA h g^{-1} at −20 °C). More importantly, they uncovered that the unpaired 3d orbital electrons in Cr play a key role in triggering the V^{4+}/V^{5+} redox couple. The fast-charging performance of $Na_3V_{1.5}Cr_{0.5}(PO_4)_3$ was explored by Lai's group.[48] They designed a reduced graphene oxide supported $Na_3V_{1.5}Cr_{0.5}(PO_4)_3$ cathode (VC/C-G) for fast sodium storage, which delivers a high specific capacity of 176 mA h g^{-1} and long cycle life. Noticeably, VC/C-G also exhibits an outstanding fast-charging performance (a short time of ~11 min to realize 80% state of charge).

Recently, V/Cr solid-solution MXene was employed as a precursor to prepare Cr-substituted NVP ($Na_3V_{1.625}Cr_{0.375}(PO_4)_3$) by a facile *in situ* reactive transformation strategy (Fig. 6a).[49] An extra voltage plateau of the V^{4+}/V^{5+} redox couple at 4.02/3.98 V was observed in $Na_3V_{1.625}Cr_{0.375}(PO_4)_3$. They found that the Na^+ ordering at Na_2 sites was changed by Cr substitution, which induces an intermediate phase during the charge/discharge process and decreases the Na^+ migration energy barriers. The Na^+ diffusion coefficient of $Na_3V_{1.625}Cr_{0.375}(PO_4)_3$ was significantly improved. As a result, the $Na_3V_{1.625}Cr_{0.375}(PO_4)_3$ electrode delivers smaller polarization (40 mV, Fig. 6b), outstanding rate performance (78.0 mA g^{-1} at 200C, Fig. 6c), long cycle life (a capacity retention of 71.5% after 1500 cycles, Fig. 6d), and high energy density (410 W h kg^{-1}) and power density (68 975 W kg^{-1}). Most recently, a $Na_3V_{4/3}Cr_{2/3}(PO_4)_3$ hollow microsphere was prepared by spray drying, which shows a high discharge capacity of 175 mA h g^{-1} and excellent cycling performance.[50]
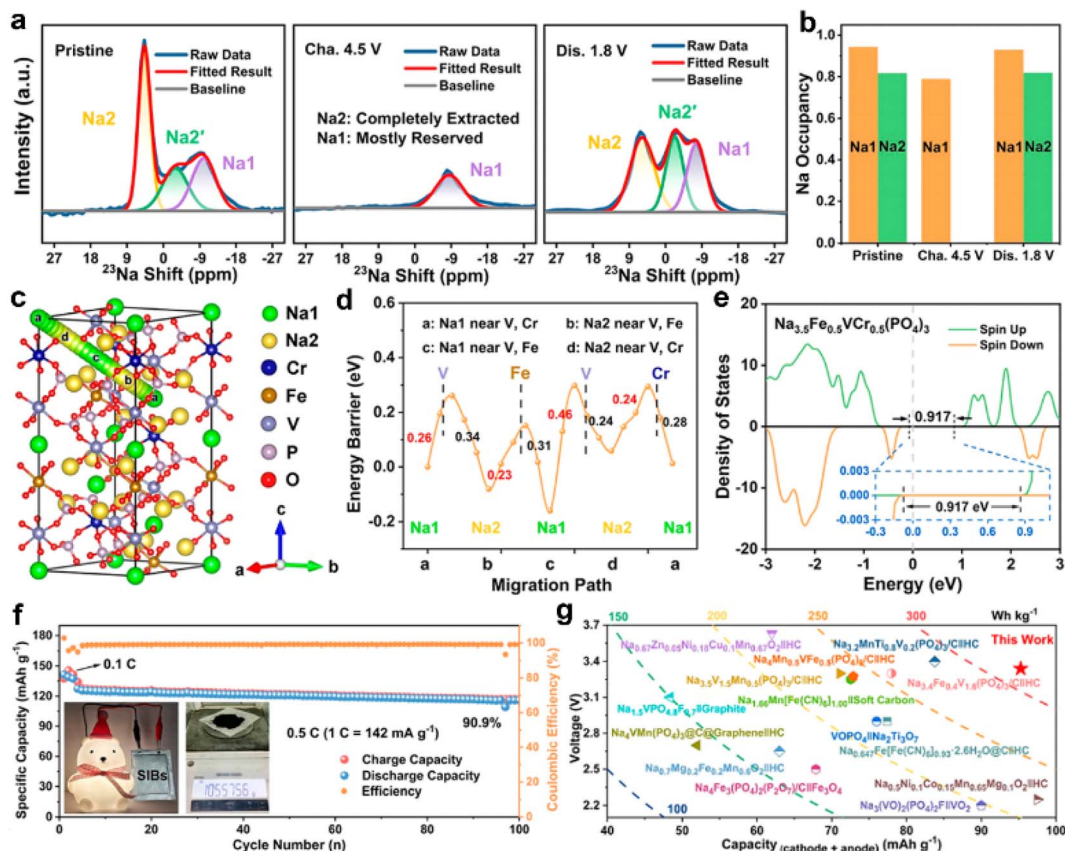
Fig. 7 (a) *Ex situ* ^{23}Na ss-NMR spectra and (b) Na occupancy results of NFVCP at various electrochemical states. (c) DFT calculations of the schematic diagram of the optimum Na$^+$ migration path in the NFVCP lattice and (d) corresponding migration energy barriers. (e) The total density of states of NFVCP. (f) Cycling stability of the NFVCP‖HC full cell. Insets show the mass production of the NFVCP cathode material and the LED bulb powered by the pouched full cell. (g) Comparison of voltage, capacity, and energy density between the NFVCP‖HC full cell and those of the state-of-the-art Na-ion full cells. Reproduced with permission.[59] Copyright 2023, American Chemical Society.

The aluminum substituted NVP with the activated V^{4+}/V^{5+} redox couple was first reported by Masquelier's group.[51] Benefiting from the lighter molecular weight of Al and high operating potential of the V^{4+}/V^{5+} redox couple, the Na$_3$Al$_{0.5}$V$_{1.5}$(PO$_4$)$_3$ achieves an improved energy density of 424.6 W h kg^{-1}. Subsequently, Lavela designed a carbon-loaded Na$_3$V$_{1.8}$Al$_{0.2}$(PO$_4$)$_3$ as a cathode material for SIBs.[52] The GITT result reveals the fast electrochemical reaction kinetics of Na$_3$V$_{1.8}$Al$_{0.2}$(PO$_4$)$_3$. Therefore, Na$_3$V$_{1.8}$Al$_{0.2}$(PO$_4$)$_3$ delivers a superior rate performance. Similarly, Criado *et al.* prepared a carbon-coated Na$_3$VAl(PO$_4$)$_3$ by a single and easily scalable sol–gel route.[53] Unfortunately, the V^{4+}/V^{5+} redox couple in Na$_3$VAl(PO$_4$)$_3$ showed an unsatisfactory reversibility.

In 2019, Chen *et al.* synthesized a series of graphene-like graphitic layer decorated Na$_3$V$_{2-x}$Ga$_x$(PO$_4$)$_3$ (x = 0, 0.1, 0.2, 0.4, and 0.6) materials *via* a solid-state reaction method.[54] Noticeably, an impurity of Ga(PO$_3$)$_3$ was generated when x reached 0.6. Na$_3$V$_{2-x}$Ga$_x$(PO$_4$)$_3$ (x = 0.1, 0.2 and 0.4) exhibited two redox peaks at 3.4 V and 4 V, which were assigned to V^{3+}/V^{4+} and V^{4+}/V^{5+} redox couples. Na$_3$V$_{1.6}$Ga$_{0.4}$(PO$_4$)$_3$ shows dramatically improved rate performance and cycling stability, a reversible capacity of 80.6 mA h g^{-1} at 50C, and a capacity retention of 97.3% after 1000 cycles. More importantly, Na$_3$V$_{1.6}$Ga$_{0.4}$(PO$_4$)$_3$

delivers a high energy density (355.5 W h kg^{-1}) and power density (11 075 W kg^{-1} at 50C). They disclosed that the Ga^{3+} substitution also benefits the enhancement of the proportion of sp^2-type carbon and boost the rate performance. Similarly, Zheng's group also demonstrated that the reversible activation of V^{4+}/V^{5+} can be realized by introducing Ga^{3+} in NVP.[55]

The reason for the different potentials of the V^{4+}/V^{5+} redox couple in Na$_3$VM(PO$_4$)$_3$ (M = Ga or Al) and Na$_3$V$_2$(PO$_4$)$_3$ was investigated by Jin's group.[31] They reveal that the potentials of the V^{4+}/V^{5+} redox couple were closely related to the crystallographic sites of sodium ion extraction/insertion. Sodium ions were extracted from the Na$_2$ site in Na$_3$VM(PO$_4$)$_3$, while it was from the Na$_1$ site in Na$_3$V$_2$(PO$_4$)$_3$. Therefore, Na$_3$VM(PO$_4$)$_3$ showed lower potentials of the V^{4+}/V^{5+} redox couple than that of Na$_3$V$_2$(PO$_4$)$_3$. In addition, they found that the excessive diffusion activation energy in Na$_3$VM(PO$_4$)$_3$ was responsible for the limited V^{4+}/V^{5+} redox reaction, therefore, a breakthrough can be realized by smaller-sized cation substitution for V^{3+}.

Noticeably, the effect of alkali metal substitution (Li, Na, and K) on the electrochemical performance of NVP-based materials was recently investigated by Wu's group.[56] They found that the trace of alkali metal substitute V can effectively improve electronic conductivity and speed up ionic diffusion. Meanwhile,
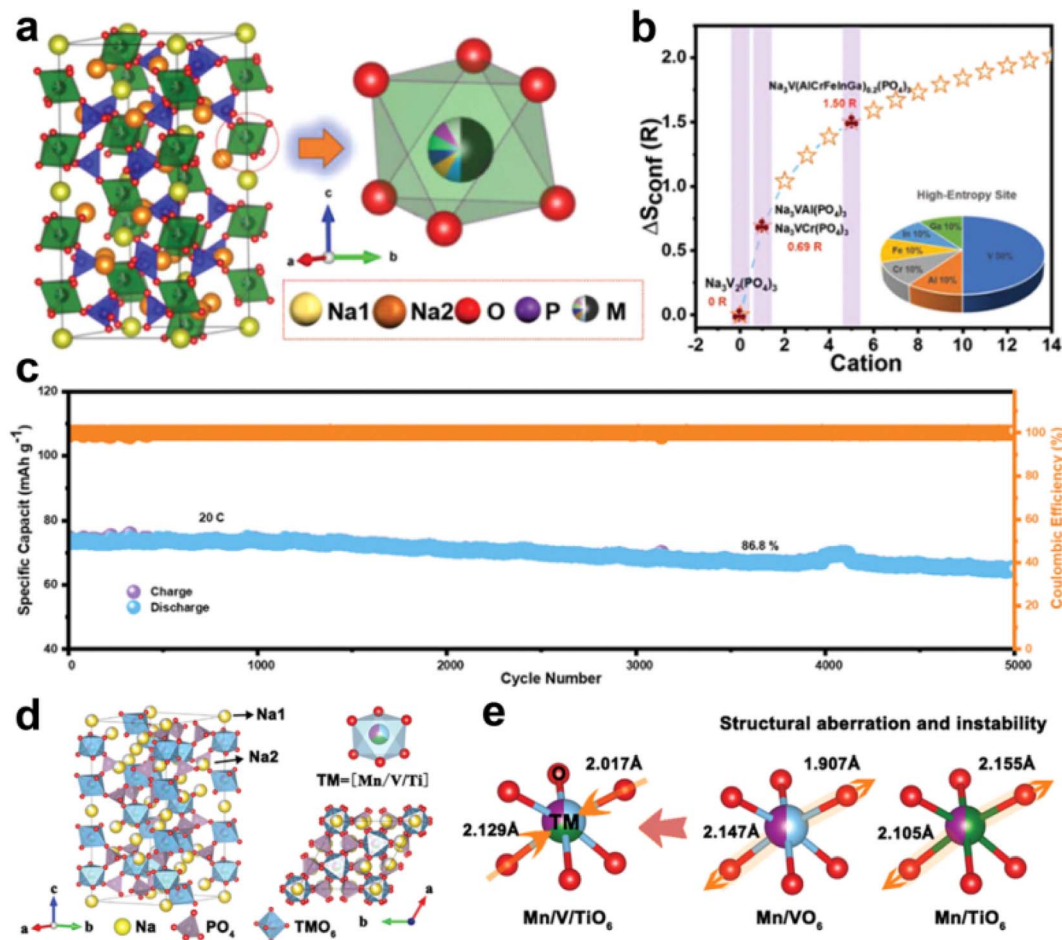
Fig. 8 (a) Schematic sketch of the NVMP crystal structure. (b) Dependence of configurational entropy on the number of cation elements. (c) Long-term cycling performance of the NVMP cathode electrode. Reproduced with permission.[65] Copyright 2023, Wiley-VCH. (d) Visualization of the crystal structure and atomic occupation of ME-NMVTP. (e) Magnifications of the TMO_6 octahedron structure in ME-NMVTP cathode materials. Reproduced with permission.[67] Copyright 2023, Wiley-VCH.

the V^{4+}/V^{5+} redox reaction was partially activated with an improved reversible capacity. Compared with $Na_3V_{1.92}Li_{0.08}(PO_4)_3$ and $Na_3V_{1.92}Na_{0.08}(PO_4)_3$, $Na_3V_{1.94}K_{0.06}(PO_4)_3$ (NVP-$K_{0.06}$) shows a higher reversible capacity, superior cycling stability and outstanding rate performance. More importantly, NVP-$K_{0.06}$ shows a good temperature tolerance, and can operate in a wide temperature range of −30–55 °C.

3.2 Bimetal substitution

The bimetal substitution strategy for NVP-based materials in SIBs was reported by Wu's group; Fe and Ni were substituents for V to obtain $Na_3Fe_{0.8}VNi_{0.2}(PO_4)_3$.[57] $Na_3Fe_{0.8}VNi_{0.2}(PO_4)_3$ with the activated V^{4+}/V^{5+} redox reaction showed a high initial discharge capacity of 163.6 mA h g^{-1}, but suffer from rapid capacity fading (only 22.9 mA h g^{-1} after 50 cycles) due to its poor structural reversibility in a wide voltage range. They also proposed that the Na^+ at the Na_2 site determines the reversibility of the V^{4+}/V^{5+} redox reaction and the cycling stability of $Na_3Fe_{0.8}VNi_{0.2}(PO_4)_3$ can be improved by adjusting the charging–discharging mode in order to have enough Na^+ in the

Na_2 site. Subsequently, Wang *et al.* designed a double-carbon-layer hierarchical structure $Na_{3.5}VMn_{0.5}Cr_{0.5}(PO_4)_3@C/rGO$ (VMC@C/rGO) for SIBs.[58] The unique double-carbon-layer hierarchical structure significantly improves the electronic conductivity and structural stability of VMC@C/rGO, enabling a reversible V^{4+}/V^{5+} redox reaction. The hierarchical VMC@C/rGO electrode realized a 2.4-electron redox reaction with a high reversible capacity (136 mA h g^{-1}), capacity retention (81% after 8000 cycles at 20C) and energy density (472 W h kg^{-1}). The VMC@C/rGO‖HC full cells also exhibited superior electrochemical performance, suggesting that the VMC@C/rGO can be a promising cathode candidate for SIBs.

Recently, Liu's group reported a low-strain $Na_{3.5}Fe_{0.5}VCr_{0.5}(PO_4)_3$ (NFVCP) for SIBs, which achieves a multi-electron reaction (2.61 electrons) based on Fe^{2+}/Fe^{3+}, $V^{3+}/V^{4+}/V^{5+}$, and Cr^{3+}/Cr^{4+} redox couples.[59] As shown in Fig. 7a and b, an unexpected reversible release/uptake of the Na^+ in the Na_1 site was observed during the charge/discharge process. In addition, *in situ* XRD reveals that the NFVCP undergoes a highly reversible bi-phase and solid-solution reaction with a small volume change of 3.87%. NFVCP also exhibits a low migration energy

Table 1 The electrochemical performance of some representative NVP-based cathode materials with activated V^{4+}/V^{5+} redox reactions

Classification	Materials	Voltage range (V versus Na^+/Na)	Initial discharge capacity (mA h g^{-1})/current density (mA g^{-1})	V^{4+}/V^{5+} contribution in total capacity/%	Rate performance (mA h g^{-1})/current density (mA g^{-1})	Cycling stability (capacity retention %/cycles)	Ref.
Single metal substitution (Fe)	$Na_{3.5}V_{1.5}Fe_{0.5}(PO_4)_3$	2.0–4.2	~90/0.5C	~11.1	~30/10C	80/300	38
	$Na_{3.4}V_{1.6}Fe_{0.4}(PO_4)_3$	2.0–4.1	133/0.5C	~16.9	~113/20C	96/2000	40
	$Na_{3.5}V_{1.5}Fe_{0.5}(PO_4)_3$	1.7–4.3	148.2/0.5C	~6.7	73.5/100C	72/500	41
Single metal substitution (Cr)	$Na_3V_{1.5}Cr_{0.5}(PO_4)_3$	1.0–4.4	~150/30	~20	~35/1000	96/400	32
	$Na_3V_{1.5}Cr_{0.5}(PO_4)_3$	1.0–4.2	163.2/0.1C	~9.2	~120/10C	72.1/2650	47
	$Na_3Cr_{0.5}V_{1.5}(PO_4)_3$		176/0.2C	~8.5	94.8/50C	~50/1000	48
	$Na_3V_{1.625}Cr_{0.375}(PO_4)_3$	2.5–4.5	122.9/1C	~16.3	78.0/200C	93.4/300	49
	$Na_3V_{4/3}Cr_{2/3}(PO_4)_3$	1.5–4.4	175/100	~14.3	94/5000	86/2000	50
Single metal substitution (Ga)	$Na_3V_{1.6}Ga_{0.4}(PO_4)_3$	2.3–4.3	105.8/0.1C	~14.2	80.6/50C	97.3/1000	54
	$Na_3V_{1.25}Ga_{0.75}(PO_4)_3$	1.4–4.2	152.3/1C		58.9/40C	84.52/600	55
Single metal substitution (Ni)	$Na_4NiV(PO_4)_3$		~80/1C		70/5C	~83/500	42
Single metal substitution (K)	$Na_3V_{1.94}K_{0.06}(PO_4)_3$	2.0–4.0	120.3/0.1C		100.5/20C	99.1/3000	56
Single metal substitution (Mn)	$Na_{3.75}V_{1.25}Mn_{0.75}(PO_4)_3$	2.75–4.2	100/1C		95/2C	61/50	43
	$Na_{3.5}VMn_{0.5}Cr_{0.5}(PO_4)_3$	2.0–4.2	136/0.2C		61.4/20C	94.7/1600 81/8000	58
Bimetal substitution	$Na_{3.5}Fe_{0.5}VCr_{0.5}(PO_4)_3$	1.8–4.5	148.5/0.1C	~10.1	88.3/50C	95.1/2000	59
	$Na_3Mn_{2/3}V_{2/3}Ti_{2/3}(PO_4)_3$	1.5–4.3	147.9/50		57.7/500	88.3/1000	67
	$Na_3Fe_{0.8}VNi_{0.2}(PO_4)_3$	1.3–4.2	161.8/0.1C	~9.3	63.1/20C	71.2/200	57
Regulation of conformational entropy	$Na_4VFe_{0.6}Mn_{0.2}Cr_{0.1}(CoMgAl)_{0.1}(PO_4)_3$	1.5–4.1	141.98/1C		85.77/50C	66.7/10 000	66
	$Na_3VAl_{0.2}Cr_{0.2}Fe_{0.2}In_{0.2}Ga_{0.2}(PO_4)_3$	2.5–4.4	102/0.1C	~22	71/20C	86.8/5000	65
	$Na_{3.32}V_{1.6}Cr_{0.08}Fe_{0.08}Mn_{0.08}Mg_{0.08}Ca_{0.08}(PO_4)_3$	1.2–4.2	152.3/50		122.3/5000	93.1/2000	69
	$Na_{3.5}V_{0.5}Mn_{0.5}Fe_{0.5}Ti_{0.5}(PO_4)_3$	1.8–4.4	165.8/0.1C		69/100C	83.5/10 000	68

barrier of 0.23–0.46 eV and a narrow band gap of 0.917 eV (Fig. 7c–e). Therefore, NFVCP shows a high reversible capacity of 148.5 mA h g^{-1} and good capacity retention of 95.1% after 2000 cycles. The potential of NFVCP for practical application was further demonstrated by the superior electrochemical performance of NFVCP‖HC full cells. NFVCP‖HC full cells delivered a good rate capability (70.9 mA h g^{-1} at 30C), low-temperature performance (77.2% of its room-temperature capacity at −20 °C) and cycling stability (a capacity retention of 90.9% after 100 cycles, Fig. 7f). More importantly, NFVCP‖HC full cells exhibit a high energy density of ~318.2 W h kg^{-1} (Fig. 7g).

3.3 Regulation of conformational entropy

In general, the increase of conformational entropy induces many possible combinations of interaction that can boost the crystal structure stability and electrochemical performance.[60–63] The conformational entropy $\geq 1.5R$ (where R is the molar gas constant) is referred to as high-entropy.[64] Materials with conformational entropy ranging from $1R$ to $1.5R$ are classified as medium-entropy, while those below $1R$ are termed low-entropy. Zhao et al. applied the concept of high entropy and constructed NASICON-type $Na_3VAl_{0.2}Cr_{0.2}Fe_{0.2}In_{0.2}Ga_{0.2}(PO_4)_3$ (NVMP) as a cathode material for SIBs (Fig. 8a and b).[65] A highly reversible V^{4+}/V^{5+} redox reaction and structural evolution with

a volume change of 1.1% during the charge/discharge process were realized in NVMP. Accordingly, the NVMP cathode offers a high reversible specific capacity of 102 mA h g^{-1} and a good rate performance (71 mA h g^{-1} at 20C). In addition, the NVMP cathode delivers superior cycling stability in a wide temperature range (capacity retention of 86.8% after 5000 cycles at room temperature (Fig. 8c) and a capacity retention of ~94.2% after 1000 cycles at −20 °C). The NVMP‖HC full cells showed a capacity retention of 93% after 50 cycles, indicating the potential of NVMP cathode materials for practical application. Similarly, Hou's group realized excellent rate capability at high voltage, and good ionic and electronic conductivity by the intrinsic effect of multiple metals in the as-prepared cathode material $Na_4VFe_{0.6}Mn_{0.2}Cr_{0.1}(CoMgAl)_{0.1}(PO_4)_3$ (NVFP-HE).[66] In addition, in situ XRD revealed that the high entropy NVFP-HE showed a highly reversible structure evolution at high voltage, therefore enabling NVFP-HE to deliver superior cycling stability (a capacity retention of 66.7% after 10 000 cycles).

The medium-entropy $Na_3Mn_{2/3}V_{2/3}Ti_{2/3}(PO_4)_3$/C@CNTs (ME-NMVTP) cathode for SIBs was reported by Wang's group (Fig. 8d and e).[67] Various redox reactions of V^{2+}/V^{3+}, Ti^{3+}/Ti^{4+}, V^{3+}/V^{4+}, Mn^{2+}/Mn^{3+}, V^{4+}/V^{5+}, and Mn^{3+}/Mn^{4+} were observed in ME-NMVTP, which achieved a high reversible capacity of 147.9 mA h g^{-1}. Benefiting from the synergistic effect of the three transition-metal elements, ME-NMVTP showed improved

electronic conductivity, accelerated Na^+ diffusion coefficient and superior structural stability with a small volume change. Both the half cell and ME-NMVTP‖HC full cell exhibited superior rate performance and cycling stability, suggesting that ME-NMVTP‖HC is a promising cathode candidate for SIBs. Similarly, Zhao's group applied a medium-entropy NASICON-structure cathode $Na_{3.5}V_{0.5}Mn_{0.5}Fe_{0.5}Ti_{0.5}(PO_4)_3$ (Me-NVMP) for SIBs.[68] *In situ* XRD discloses that the Me-NVMP shows a solid-solution-type Na^+ storage behavior. In addition, Me-NVMP can effectively inhibit the undesirable Jahn–Teller distortion and irreversible structural evolution at high voltage. Therefore, Me-NVMP shows a high reversible capacity (165.8 mA h g^{-1}) and superior cycling stability (a high capacity retention of 83.5% even after 10 000 cycles).

Most recently, Chou's group proposed a strategy that combines high-entropy substitution and electrolyte optimization to boost the reversible multielectron reactions of NVP.[69] *In situ* X-ray absorption near-edge structure spectra and *in situ* XRD demonstrated the high reversibility of the V^{5+}/V^{4+} redox couple and crystalline structure evolution. Therefore, $Na_{3.32}V_{1.6}Cr_{0.08}Fe_{0.08}Mn_{0.08}Mg_{0.08}Ca_{0.08}(PO_4)_3$ (HE-V$_{1.6}$) delivers a high capacity retention of 93.1% after 2000 cycles. Meanwhile, HE-V$_{1.6}$ shows a good temperature tolerance; it maintains a stable operation in a wide temperature range (-20 to $60\ °C$). More importantly, the HE-V$_{1.6}$‖natural graphite full cell was assembled to demonstrate the potential of HE-V$_{1.6}$ for practical application, which shows a high power density and long cycle life. These results reveal that HE-V$_{1.6}$ is a promising candidate for high-performance SIBs.

4. Conclusions and perspectives

NVP-based cathode materials with activated V^{4+}/V^{5+} redox reactions have been considered as promising candidates for high energy density SIBs. In this review, we systematically discuss the emerging high voltage V^{4+}/V^{5+} redox reaction in NVP-based cathodes, including their faced challenges and recent achievements. In general, the NVP-based cathode material with the activated V^{4+}/V^{5+} redox reaction suffers from low electronic conductivity and inferior structure reversibility at high voltage. Meanwhile, transition metal substitution was demonstrated as an effective strategy to activate the V^{4+}/V^{5+} redox reaction in NVP-based cathode materials. To better understand the superiority of the NVP-based cathode material with the activated V^{4+}/V^{5+} redox reaction, the electrochemical performance of some representative materials is summarized in Table 1.

To achieve the practical application of NVP-based cathode materials with activated V^{4+}/V^{5+} redox reactions, we suggested that further research should be focused on the following aspects. First, the inert or low redox potential of transition metal substitution inevitably leads to a decrease in the number of active redox centers or operating voltage, resulting in an unsatisfactory energy density. Artificial intelligence can be used as a suitable tool to screen novel high-performance NVP-based cathode materials with activated V^{4+}/V^{5+} redox reactions to boost the energy density of SIBs. Second, the electrode/

electrolyte interphase plays a key role in the electrochemical performance of high-voltage electrode materials, exploring an electrolyte with good compatibility to construct a robust electrode/electrolyte interphase and improve sodium storage performance is very meaningful. Third, the intrinsic low electronic conductivity and poor structural reversibility of NVP-based cathode materials inevitably limit their electrochemical performance. Therefore, in order to elevate electronic conductivity and alleviate volume change, the development of NVP-based cathode materials with high conductivity coating layers and unique morphology might be a significant approach. Fourth, exploring the effects of composition on electrochemical performance is of vital importance. Fifth, the mechanism of activating V^{4+}/V^{5+} redox reactions in NVP-based electrode materials is not clear; it is necessary to get further understanding of the mechanism by both advanced *in situ* characterization techniques and theoretical calculations. Finally, the potential of cathode materials for SIBs should be evaluated in full cells and pouch cells.

Author contributions

Conflicts of interest

There are no conflicts to declare.

Acknowledgements

References

1 M. Li, J. Lu, Z. Chen and K. Amine, *Adv. Mater.*, 2018, **30**, 1800561.
2 Z. Fan, X. Zhou, J. Qiu, Z. Yang, C. Lei, Z. Hao, J. Li, L. Li, R. Zeng and S. Chou, *Angew. Chem., Int. Ed.*, 2023, **62**, e202308888.
3 T. Jin, H. Li, K. Zhu, P. Wang, P. Liu and L. Jiao, *Chem. Soc. Rev.*, 2020, **49**, 2342–2377.
4 Y. You and A. Manthiram, *Adv. Energy Mater.*, 2017, **8**, 1701785.

5 X. Zhou, Y. Huang, B. Wen, Z. Yang, Z. Hao, L. Li, S. Chou and F. Li, *Proc. Natl. Acad. Sci. U. S. A.*, 2024, **121**, e2316914121.

6 J. Y. Hwang, S. T. Myung and Y. K. Sun, *Chem. Soc. Rev.*, 2017, **46**, 3529–3614.

7 X. Zhou, X. Chen, Z. Yang, X. Liu, Z. Hao, S. Jin, L. Zhang, R. Wang, C. Zhang, L. Li, X. Tan and S. Chou, *Adv. Funct. Mater.*, 2024, **34**, 2302281.

8 Y. Liao, L. Yuan, Y. Han, C. Liang, Z. Li, Z. Li, W. Luo, D. Wang and Y. Huang, *Adv. Mater.*, 2024, **36**, 2312287.

9 Z. Yang, X. Zhou, Z. Hao, J. Chen, L. Li, Q. Zhao, W. Lai and S. Chou, *Angew. Chem., Int. Ed.*, 2024, **63**, e202313142.

10 Z. Tang, R. Zhang, H. Wang, S. Zhou, Z. Pan, Y. Huang, D. Sun, Y. Tang, X. Ji, K. Amine and M. Shao, *Nat. Commun.*, 2023, **14**, 6024.

11 Y. Yang, C. Wu, X.-X. He, J. Zhao, Z. Yang, L. Li, X. Wu, L. Li and S.-L. Chou, *Adv. Funct. Mater.*, 2024, **34**, 2302277.

12 S. Chu, D. Kim, G. Choi, C. Zhang, H. Li, W. Pang, Y. Fan, A. M. D'Angelo, S. Guo and H. Zhou, *Angew. Chem., Int. Ed.*, 2023, **62**, e202216174.

13 T. Song, C. Wang and C.-S. Lee, *Carbon Neutralization*, 2022, **1**, 68–92.

14 A. K. Paidi, W. B. Park, P. Ramakrishnan, S. H. Lee, J. W. Lee, K. S. Lee, H. Ahn, T. Liu, T. Gim, M. Avdeev, M. Pyo, J. I. Sohn, K. Amine, K. S. Sohn, T. J. Shin, D. Ahn and J. Lu, *Adv. Mater.*, 2022, **34**, 2202137.

15 H. Fu, Y. Wang, G. Fan, S. Guo, X. Xie, X. Cao, B. Lu, M. Long, J. Zhou and S. Liang, *Chem. Sci.*, 2022, **13**, 726–736.

16 Z. Hao, X. Shi, Z. Yang, X. Zhou, L. Li, C. Ma and S. Chou, *Adv. Mater.*, 2024, **36**, 2305135.

17 J. Guo, H. Zhang, Z. Gu, M. Du, H. Lü, X. Zhao, J. Yang, W. Li, S. Kang, W. Zou and X. Wu, *Adv. Funct. Mater.*, 2022, **32**, 2209482.

18 Y. Qi, Z. Tong, J. Zhao, L. Ma, T. Wu, H. Liu, C. Yang, J. Lu and Y. Hu, *Joule*, 2018, **2**, 2348–2363.

19 M. Xu, F. Zhang, Y. Zhang, C. Wu, X. Zhou, X. Ai and J. Qian, *Chem. Sci.*, 2023, **14**, 12570–12581.

20 C. Xu, Y. Ma, J. Zhao, P. Zhang, Z. Chen, C. Yang, H. Liu and Y.-S. Hu, *Angew. Chem., Int. Ed.*, 2023, **62**, e202217761.

21 H. Zhang, J. Peng, L. Li, Y. Zhao, Y. Gao, J. Wang, Y. Cao, S. Dou and S. Chou, *Adv. Funct. Mater.*, 2023, **33**, 2210725.

22 E. J. Kim, T. Hosaka, P. R. Kumar, Z. T. Gossage, R. Tatara, S. Komaba and K. Kubota, *Chem. Sci.*, 2022, **13**, 6121–6158.

23 C. Wang, Y. Fang, Y. Xu, L. Liang, M. Zhou, H. Zhao and Y. Lei, *Adv. Funct. Mater.*, 2016, **26**, 1777–1786.

24 G. Zhou, Y. Miao, Z. Wei, L. Mo, F. Lai, Y. Wu, J. Ma and T. Liu, *Adv. Funct. Mater.*, 2018, **28**, 1804629.

25 Y. Lu, Q. Zhang, L. Li, Z. Niu and J. Chen, *Chem*, 2018, **4**, 2786–2813.

26 Y. Niu, Y. Zhao and M. Xu, *Carbon Neutralization*, 2023, **2**, 150–168.

27 H. Pan, Y. Hu and L. Chen, *Energy Environ. Sci.*, 2013, **6**, 2338–2360.

28 Y. Liu, X. Wu, A. Moeez, Z. Peng, Y. Xia, D. Zhao, J. Liu and W. Li, *Adv. Energy Mater.*, 2023, **13**, 2203283.

29 Y. Jiang, X. Zhou, D. Li, X. Cheng, F. Liu and Y. Yu, *Adv. Energy Mater.*, 2018, **8**, 1800068.

30 G. Chen, Q. Huang, T. Wu and L. Lu, *Adv. Funct. Mater.*, 2020, **30**, 2001289.

31 Q. Wang, H. Gao, J. Li, G. Liu and H. Jin, *ACS Appl. Mater. Interfaces*, 2021, **13**, 14312–14320.

32 Y. Zhao, X. Gao, H. Gao, H. Jin and J. B. Goodenough, *Adv. Funct. Mater.*, 2020, **30**, 1908680.

33 T. I. Perfilyeva, A. M. Alekseeva, O. A. Drozhzhin and E. V. Antipov, *Russ. J. Electrochem.*, 2023, **59**, 481–488.

34 S. Y. Lim, H. Kim, R. A. Shakoor, Y. Jung and J. W. Choi, *J. Electrochem. Soc.*, 2012, **159**, A1393–A1397.

35 R. Liu, S. Zheng, Y. Yuan, P. Yu, Z. Liang, W. Zhao, R. Shahbazian-Yassar, J. Ding, J. Lu and Y. Yang, *Adv. Energy Mater.*, 2020, **11**, 2003256.

36 F. Chen, V. M. Kovrugin, R. David, O. Mentré, F. Fauth, J. N. Chotard and C. Masquelier, *Small Methods*, 2018, **3**, 1800218.

37 M. J. Aragón, P. Lavela, G. F. Ortiz and J. L. Tirado, *J. Electrochem. Soc.*, 2015, **162**, A3077–A3083.

38 B. M. de Boisse, J. Ming, S. Nishimura and A. Yamada, *J. Electrochem. Soc.*, 2016, **163**, A1469–A1473.

39 M. Hadouchi, N. Yaqoob, P. Kaghazchi, M. Tang, J. Liu, P. Sang, Y. Fu, Y. Huang and J. Ma, *Energy Storage Mater.*, 2021, **35**, 192–202.

40 C. Xu, J. Zhao, Y. Wang, W. Hua, Q. fu, X. Liang, X. Rong, Q. Zhang, X. Guo, C. Yang, H. Liu, B. Zhong and Y. Hu, *Adv. Energy Mater.*, 2022, **12**, 2200966.

41 Y. Zhou, G. Xu, J. Lin, Y. Zhang, G. Fang, J. Zhou, X. Cao and S. Liang, *Adv. Mater.*, 2023, **35**, 2304428.

42 W. Zhou, L. Xue, X. Lu, H. Gao, Y. Li, S. Xin, G. Fu, Z. Cui, Y. Zhu and J. B. Goodenough, *Nano Lett.*, 2016, **16**, 7836–7841.

43 S. Ghosh, N. Barman, M. Mazumder, S. K. Pati, G. Rousse and P. Senguttuvan, *Adv. Energy Mater.*, 2019, **10**, 1902918.

44 A. Inoishi, Y. Yoshioka, L. Zhao, A. Kitajou and S. Okada, *ChemElectroChem*, 2017, **4**, 2755–2759.

45 M. J. Aragón, P. Lavela, G. F. Ortiz and J. L. Tirado, *ChemElectroChem*, 2015, **2**, 995–1002.

46 R. Liu, G. Xu, Q. Li, S. Zheng, G. Zheng, Z. Gong, Y. Li, E. Kruskop, R. Fu, Z. Chen, K. Amine and Y. Yang, *ACS Appl. Mater. Interfaces*, 2017, **9**, 43632–43639.

47 M. Chen, W. Hua, J. Xiao, J. Zhang, V. W. Lau, M. Park, G. H. Lee, S. Lee, W. Wang, J. Peng, L. Fang, L. Zhou, C. K. Chang, Y. Yamauchi, S. Chou and Y. M. Kang, *J. Am. Chem. Soc.*, 2021, **143**, 18091–18102.

48 W. Zhang, Y. Wu, Z. Xu, H. Li, M. Xu, J. Li, Y. Dai, W. Zong, R. Chen, L. He, Z. Zhang, D. J. L. Brett, G. He, Y. Lai and I. P. Parkin, *Adv. Energy Mater.*, 2022, **12**, 2201065.

49 H. Yu, X. Ruan, J. Wang, Z. Gu, Q. Liang, J. Cao, J. Kang, C. Du and X. Wu, *ACS Nano*, 2022, **16**, 21174–21185.

50 B. Mai, B. Xing, Y. Yue, N. Cai, C. Cai, S. Lian, H. Fan, M. Yan, T. Zhu, P. Hu, X. Wang and L. Mai, *J. Mater. Sci. Technol.*, 2023, **165**, 1–7.

51 F. Lalère, V. Seznec, M. Courty, R. David, J. N. Chotard and C. Masquelier, *J. Mater. Chem. A*, 2015, **3**, 16198–16205.

52 M. J. Aragón, P. Lavela, R. Alcántara and J. L. Tirado, *Electrochim. Acta*, 2015, **180**, 824–830.

53 A. Criado, P. Lavela, J. L. Tirado and C. Perez-Vicente, *ACS Appl. Mater. Interfaces*, 2020, **12**, 21651–21660.

54 Q. Hu, J. Liao, X. He, S. Wang, L. Xiao, X. Ding and C. Chen, *J. Mater. Chem. A*, 2019, **7**, 4660–4667.

55 Y. Chen, X. Liao, P. Wang, J. Chen, X. Zhang, X. Wu, S. C. Smith, D. Lin, X. Tan and Q. Zheng, *J. Colloid Interface Sci.*, 2024, **653**, 1–10.

56 X. Shen, M. Han, Y. Su, M. Wang and F. Wu, *Nano Energy*, 2023, **114**, 108640.

57 Q. Zhao, J. Li, M. Chen, H. Wang, Y. Xu, X. Wang, X. Ma, Q. Wu, X. Wu and X. Zeng, *Nano Lett.*, 2022, **22**, 9685–9692.

58 J. Wang, L. Zhao and F. Lu, *Adv. Mater.*, 2023, **4**, 1998–2007.

59 H. Li, Y. Wang, X. Zhao, J. Jin, Q. Shen, J. Li, Y. Liu, X. Qu, L. Jiao and Y. Liu, *ACS Energy Lett.*, 2023, **8**, 3666–3675.

60 K. Tian, H. He, X. Li, D. Wang, Z. Wang, R. Zheng, H. Sun, Y. Liu and Q. Wang, *J. Mater. Chem. A*, 2022, **10**, 14943–14953.

61 Y. Ma, Y. Ma, S. L. Dreyer, Q. Wang, K. Wang, D. Goonetilleke, A. Omar, D. Mikhailova, H. Hahn, B. Breitung and T. Brezesinski, *Adv. Mater.*, 2021, **33**, e2101342.

62 H. Li, M. Xu, H. Long, J. Zheng, L. Zhang, S. Li, C. Guan, Y. Lai and Z. Zhang, *Adv. Sci.*, 2022, **9**, e2202082.

63 K. Wang, Z. Zhang, S. Cheng, X. Han, J. Fu, M. Sui and P. Yan, *eScience*, 2022, **2**, 529–536.

64 Y. Yao, Q. Dong, A. Brozena, J. Luo, J. Miao, M. Chi, C. Wang, I. G. Kevrekidis, Z. J. Ren, J. Greeley, G. Wang, A. Anapolsky and L. Hu, *Science*, 2022, **376**, eabn3103.

65 M. Li, C. Sun, Q. Ni, Z. Sun, Y. Liu, Y. Li, L. Li, H. Jin and Y. Zhao, *Adv. Energy Mater.*, 2023, **13**, 2203971.

66 M. T. Ahsan, D. Qiu, Z. Ali, Z. Fang, W. Zhao, T. Shen and Y. Hou, *Adv. Energy Mater.*, 2024, **14**, 2302733.

67 L. Zhu, M. Wang, S. Xiang, D. Sun, Y. Tang and H. Wang, *Adv. Energy Mater.*, 2023, **13**, 2302046.

68 M. Li, C. Sun, X. Yuan, Y. Li, Y. Yuan, H. Jin, J. Lu and Y. Zhao, *Adv. Funct. Mater.*, 2024, DOI: **10.1002/adfm.202314019**.

69 Z. Hao, X. Shi, W. Zhu, Z. Yang, X. Zhou, C. Wang, L. Li, W. Hua, C. Ma and S. Chou, *ACS Nano*, 2024, **18**, 9354–9364.